

Nambu–Jona-Lasinio $SU(3)$ model constrained by lattice QCD: thermomagnetic effects in the magnetization

William R. Tavares^{c,1}, Ricardo L. S. Farias^{b,2}, Sidney S. Avancini^{a,1},
Varese S. Timóteo^{d,3}, Marcus B. Pinto^{e,1}, Gastão Krein^{f,4}

¹Departamento de Física, Universidade Federal de Santa Catarina, 88040-900 Florianópolis, SC, Brazil

²Departamento de Física, Universidade Federal de Santa Maria, 97105-900 Santa Maria, RS, Brazil

³Grupo de Óptica e Modelagem Numérica, Faculdade de Tecnologia, Universidade Estadual de Campinas, 13484-332 Limeira, SP, Brazil

⁴Instituto de Física Teórica, Universidade Estadual Paulista, Rua Dr. Bento Teobaldo Ferraz, 271 - Bloco II, 01140-070 São Paulo, SP, Brazil

Received: date / Accepted: date

Abstract We use a three-flavor Nambu–Jona-Lasinio model to study the thermodynamics of strange quark matter under a strong magnetic field. The model Lagrangian features flavor $SU(3)$ four-quark interactions and six-quark interactions that break the $U_A(1)$ symmetry. We incorporate thermomagnetic effects in the four-quark coupling by fitting lattice results for the average of u and d quark condensates close to the pseudocritical temperature. We compute the pressure at the mean field level and obtain the magnetization of quark matter. We adopt the recently proposed vacuum magnetic regularization (VMR) scheme, in that divergent quark mass independent contributions are not subtracted, thereby avoiding unphysical results for the magnetization. We devote special attention to the renormalized magnetization, a projected quantity that allows for direct comparisons with lattice QCD simulations. Our results are in very good agreement with lattice data indicating a paramagnetic behavior for quark matter.

1 Introduction

The possible existence of strong magnetic fields in non-central heavy-ion collisions [1–3], magnetars [4, 5] and the early universe [6, 7] is the topic of several recent studies. The interest is steered by the impact strong magnetic fields can have on prominent quantum-chromodynamics (QCD) phenomena, notably those related to QCD’s approximate chiral symmetry in the light-quark

sector. Phenomena such as the chiral magnetic effect [2, 8], chiral separation effect [9], chiral Alfvén wave [10] among several others are the subject of intense theoretical and experimental studies [11, 12]. The vast majority of the theoretical studies of such phenomena are carried out with effective models and theories—Refs. [13–15] are recent reviews containing extensive lists of references. Such studies received a boost when *ab initio* lattice QCD (LQCD) results [16, 17] revealed an unexpected behavior of the chiral quark condensate as a function of the magnetic field strength (B), namely: at low temperatures the condensate increases with B , characterizing magnetic catalysis (MC), whereas close to the pseudocritical temperature of the QCD transition the condensate decreases with B , characterizing inverse magnetic catalysis (IMC). The unexpected relates to the latter, as all effective models and earlier LQCD studies would predict MC but not IMC. The failure of earlier LQCD studies is presently understood as being due to the use of large pion masses, much heavier than the physical mass [18, 19]. To incorporate the IMC effect within effective quark models, several ideas have been proposed [14] (see [20, 21] for recent reviews). For instance, one simple way to conciliate LQCD predictions with those from effective theories, mostly in the context of those related to the Nambu–Jona-Lasinio model [22, 23], is to adopt a thermomagnetic dependent coupling [24, 25] constrained by the LQCD results of the average chiral condensates [17]. Other ways to fix the coupling can be found in Refs. [26–31].

Another property observed in LQCD [32–36] and low energy effective models [33, 37–39] studies, concerns the paramagnetic nature of the QCD matter. Under a strong magnetic field, the response of QCD matter is given by the magnetization, $\mathcal{M} = \partial P / \partial(eB)$, where P

^ae-mail: william.tavares@posgrad.ufsc.br

^be-mail: ricardo.farias@ufsm.br

^ce-mail: sidney.avancini@ufsc.br

^de-mail: varese@g.unicamp.br

^ee-mail: marcus.benghi@ufsc.br

^fe-mail: gastao.krein@unesp.br

is the pressure; when $\mathcal{M} > 0$, one has paramagnetism. This characteristics can induce matter paramagnetic squeezing in non-central HICs, a phenomenon that can be observed in the elliptic flow v_2 [40]. We advocate that to study physical quantities that are explicitly B dependent, such as the renormalized magnetization [32, 40], apart from the incorporation of a thermomagnetic coupling, one also needs to adopt an adequate regularization prescription to avoid unphysical phenomena. A regularization method such as the well-known magnetic field independent regularization (MFIR) scheme [41–53], although adequate to describe chiral transitions, leads to unphysical predictions for \mathcal{M} . The source of the problem is that in the MFIR scheme, one also subtracts mass independent divergent contributions (which explicitly depend on B) that are crucial for the regularization of \mathcal{M} . To avoid this problem, Ref. [54] proposed a new regularization prescription, dubbed vacuum magnetic regularization (VMR). In that work, the VMR was proposed in the context of the two flavor NJL model, enforcing IMC by considering the magnetic dependent coupling $G(B)$ proposed in Ref. [28].

In the present paper we generalize the VMR scheme to the more realistic three flavor version of the NJL theory. We consider a model Lagrangian that features three-flavor symmetry and breaks the $U_A(1)$ symmetry; the underlying theory contains four-quark interactions with a coupling constant G and t' Hooft six-quark interactions with a coupling constant K . In this first study, we enforce IMC by considering a thermomagnetic four-quark $G = G(eB, T)$ and leave the six-quark coupling K independent of B and T . The present work suggests that the VMR scheme in conjunction with a running $G(eB, T)$ improves substantially the description of \mathcal{M} within the NJL framework. To the best of our knowledge, this work is the first study, in the context of a flavor $SU(3)$ NJL model, of QCD matter under a strong magnetic field featuring IMC and paramagnetism. We organize the presentation as follows. In Sec. 2 we present the model in the presence of a constant magnetic field. The same section contains the thermodynamical potential and the gap equations at the mean field level. Next, in Sec. 3, we present the details of the thermomagnetic running coupling together with the renormalized magnetization. Numerical results are presented in Sec. 4. We conclude and discuss perspectives of future work in Sec. 5.

2 The model

There exist several options for NJL-type of Lagrangians that feature three-flavor symmetry and break the unwanted $U_A(1)$ symmetry [55–57]. We use the one first

written down in Ref. [58]; it comprises flavor $U_L(3) \otimes U_R(3)$ symmetric four-fermion interactions and a six-point interaction that breaks the $U_A(1)$ symmetry, given by the 't Hooft determinant:

$$\mathcal{L}_{sym} = G \sum_{a=0}^8 \left[(\bar{\psi} \lambda_a \psi)^2 + (\bar{\psi} i \gamma_5 \lambda_a \psi)^2 \right], \quad (1)$$

$$\mathcal{L}_{det} = -K \left[\det \bar{\psi} (1 + \gamma_5) \psi + \det \bar{\psi} (1 - \gamma_5) \psi \right]. \quad (2)$$

Here, ψ represents the three-flavor multiplet of Dirac spinors $\psi = (\psi_u, \psi_d, \psi_s)^T$, and $\lambda^a, a = 1, \dots, 8$ are the $SU(3)$ Gell-Mann matrices and $\lambda^0 = \sqrt{3/8} I$, with I the 3×3 unit matrix. The determinant is in flavor space, it can be written in terms of the Levi-Civita tensor ϵ_{ijk} as $\det \bar{\psi} \mathcal{O} \psi = \sum_{i,j,k} \epsilon_{ijk} (\bar{\psi}_u \mathcal{O} \psi_i) (\bar{\psi}_d \mathcal{O} \psi_j) (\bar{\psi}_s \mathcal{O} \psi_k)$ with $i, j, k = u, d, s$ and $\mathcal{O} = (1 \pm \gamma_5)$. The complete Lagrangian density includes an explicit symmetry-breaking mass term and the coupling of an electromagnetic field [47]:

$$\mathcal{L} = \bar{\psi} [i \gamma_\mu D^\mu - \hat{m}] \psi + \mathcal{L}_{sym} + \mathcal{L}_{det} - \frac{1}{4} F^{\mu\nu} F_{\mu\nu}, \quad (3)$$

where $D^\mu = \partial^\mu + iQ A^\mu$, with A^μ being the electromagnetic gauge field potential and $F_{\mu\nu}$ the corresponding field tensor, Q is the quark charge matrix $Q = \text{diag}(q_u, q_d, q_s) = \text{diag}(2/3 e, -1/3 e, -1/3 e)$ where $e = \sqrt{4\pi/137}$ is the elementary electric charge, and m the current-quark mass matrix $m = \text{diag}(m_u, m_d, m_s)$. We choose a spatially uniform, time independent magnetic field of strength B pointing in the \hat{z} direction, so that one can choose the gauge field as $A^\mu = x B \delta^{\mu 2}$.

The mean-field grand-canonical potential $\Omega(T, eB)$ of the model was computed in Ref. [47] within the MFIR prescription, but one can readily transcribe that derivation to the VMR prescription [54]. In both prescriptions, the generic form of $\Omega(T, eB)$ can be written as

$$\Omega(T, eB) = \sum_f \omega_f + 2G \sum_f \phi_f^2 - 4K \phi_u \phi_d \phi_s, \quad (4)$$

where ω_f , $f = u, d, s$ comes from the first term in the Lagrangian and ϕ_f is the flavor f quark condensate that comes from the quark-quark interactions. Both ω_f and ϕ_f can be written as sum of terms with well defined origin: vacuum, purely magnetic and medium (mixed temperature and magnetic field). The differences between the MFIR and VMR appear in the expression for ω_f . Specifically, the VMR ω_f can be written as [54]:

$$\omega_f = \omega_f^{vac} + \omega_f^{mag} + \omega_f^{field} + \omega_f^{med}, \quad (5)$$

where

$$\omega_f^{vac} = \frac{N_c}{8\pi^2} \left[M_f^4 \log \left(\frac{\Lambda + \epsilon_f}{M_f} \right) - \epsilon_f \Lambda (\Lambda^2 + \epsilon_f^2) \right], \quad (6)$$

$$\omega_f^{mag} = -\frac{N_c(|q_f|B)^2}{2\pi^2} \left[\zeta'(-1, x_f) + \frac{1}{4}x_f^2 - \frac{1}{2}(x_f^2 - x_f) \log x_f - \frac{1}{12}(1 + \log x_f) \right], \quad (7)$$

$$\omega_f^{field} = -\frac{N_c(|q_f|B)^2}{24\pi^2} \log \left(\frac{M_f^2}{\Lambda^2} \right), \quad (8)$$

$$\omega_f^{med} = -T \sum_{k=0}^{\infty} (2 - \delta_{0k}) \frac{|q_f|B}{2\pi^2} \times \int_{-\infty}^{\infty} dp \ln \left(1 + e^{-E_f/T} \right), \quad (9)$$

where $\zeta'(-1, x_f) = \frac{d\zeta(z, x_f)}{dz} \Big|_{z=-1}$.

The MFIR expressions differ from the above by the absence of the last term in Eq. (7) and the ω_f^{field} contribution in Eq. (8). As mentioned, those terms are essential for describing the SU(2) lattice data. In the above expressions, we defined $\epsilon_f = (\Lambda^2 + M_f^2)^{1/2}$ where Λ is a three-dimensional cutoff, $x_f = M_f^2/2|q_f|B$, $\zeta(s, x)$ is the Riemann-Hurwitz zeta function, and $E_f = (p^2 + M_f^2 + 2|q_f|Bk)^{1/2}$. In the previous definitions, M_f represents the flavor f constituent quark mass, determined by the familiar NJL gap equations:

$$M_u = m_u - 4G\phi_u + 2K\phi_d\phi_s, \quad (10)$$

$$M_d = m_d - 4G\phi_d + 2K\phi_u\phi_s, \quad (11)$$

$$M_s = m_s - 4G\phi_s + 2K\phi_u\phi_d. \quad (12)$$

In this first study only the coupling G is enforced to be T and B dependent. As mentioned above, the flavor f quark condensate can also be expressed as a sum of vacuum, magnetic field and medium contributions, namely:

$$\phi_f = \phi_f^{vac} + \phi_f^{mag} + \phi_f^{med}, \quad (13)$$

where

$$\phi_f^{vac} = -\frac{N_c M_f}{2\pi^2} \left[\Lambda \epsilon_\Lambda - M_f^2 \log \left(\frac{\Lambda + \epsilon_\Lambda}{M_f} \right) \right], \quad (14)$$

$$\phi_f^{mag} = -\frac{M_f N_c |q_f|B}{2\pi^2} \left[\log \Gamma(x_f) - \frac{1}{2} \log(2\pi) + x_f - \frac{1}{2}(2x_f - 1) \log x_f \right], \quad (15)$$

$$\phi_f^{med} = \sum_{k=0}^{\infty} (2 - \delta_{0k}) \frac{|q_f|B N_c M_f}{2\pi^2} \times \int_{-\infty}^{\infty} dp \frac{1}{E_f} \frac{1}{e^{E_f/T} + 1}, \quad (16)$$

where Γ is the Euler gamma function.

3 Running coupling and magnetization

We use the average quark condensate $(\Sigma_u + \Sigma_d)/2$ [17] to adjust the running coupling $G(eB, T)$. To this end, we adopt the following parametrization of the Gell-Mann-Oakes-Renner (GOR) relation [17, 25]

$$\Sigma_f = \frac{2m}{m_\pi^2 f_\pi^2} \left[\langle \bar{\psi}_f \psi_f \rangle_{B,T} - \langle \bar{\psi}_f \psi_f \rangle_{00} \right] + 1, \quad (17)$$

where $\langle \bar{\psi}_f \psi_f \rangle_{00}^{1/3} = -230.55$ MeV is the quark chiral condensate at $B = T = 0$, $f_\pi = 86$ MeV, $m_\pi = 135$ MeV, and $m = 5.5$ MeV. Adopting this particular set of phenomenological values will allow us to perform direct comparisons with the lattice results of Ref. [17].

The T and B dependent condensates $\langle \bar{\psi}_f \psi_f \rangle_{B,T} = \phi_f$ are evaluated within the NJL expressions given in the previous section, Eqs. (13)-(16). The constituent quark masses M_u, M_d , and M_s in the expressions for ϕ_f are obtained by solving the gap equations Eqs. (10)-(12). The T and B running of the coupling $G = G(eB, T)$ is dictated by an *ansatz* similar to that used for the SU(2) model [25], namely:

$$G(eB, T) = \alpha(eB) \left(1 - \frac{d(eB)}{1 + e^{\beta(eB)(T_a(eB)-T)}} \right) + s(eB). \quad (18)$$

This expression has been adopted for mere convenience since it is well adapted for the adjustment of LQCD results. Of course, other possibilities may be used with similar results.

Table 1 Values of parameters in Eq.(18) in appropriate GeV units; $d(B)$ is dimensionless.

eB	$\alpha(eB)$	$\beta(eB)$	$T_a(eB)$	$d(eB)$	$s(eB)$
0.0	2.1534	420.95	0.1678	0.3506	2.0793
0.2	1.7571	142.44	0.1844	1.4636	2.3358
0.4	0.8158	183.46	0.1712	2.0641	2.8016
0.6	0.7148	128.16	0.1720	3.2874	2.3080

Table 1 displays the numerical values for the parameters appearing in Eq. (18). These selected values are those which best fit the average quark condensate. Since Ref. [17] offers no data points between $T \in [0, 113\text{MeV}]$, we follow the strategy of Ref. [25], in that we fit G using the available lattice data to extrapolate the results to lower temperatures.

In the next section we present the fitting results of the lattice data for $(\Sigma_u + \Sigma_d)/2$ [17] and compare the predictions of the model for the pseudocritical temperature with the corresponding lattice results. We will

also show results for the renormalized magnetization, \mathcal{M}^r [32, 54]:

$$\mathcal{M}^r \cdot eB = \mathcal{M} \cdot eB - (eB)^2 \lim_{eB \rightarrow 0} \frac{\mathcal{M} \cdot eB}{(eB)^2} \Big|_{T=0}, \quad (19)$$

where $\mathcal{M} = -\partial\Omega(T, eB)/\partial(eB)$, with $\Omega(T, eB)$ representing the thermodynamical potential, Eq.(4). Although the NJL model is a nonrenormalizable field theory, this prescription, which motivated the VMR for the SU(2) NJL model, gives us the possibility to compare our results directly with the LQCD data—see Ref. [54] for more details.

4 Numerical results

The following set of parameters is adopted in this work: $\Lambda = 631.4$ MeV, $m_u = m_d = 5.5$ MeV, $m_s = 135.7$ MeV, $G = 1.835/\Lambda^2$ and $K = 9.29/\Lambda^5$ [57]. We note that the value of G corresponds to the vacuum value, not the extrapolated $G(B = 0, T = 0)$.

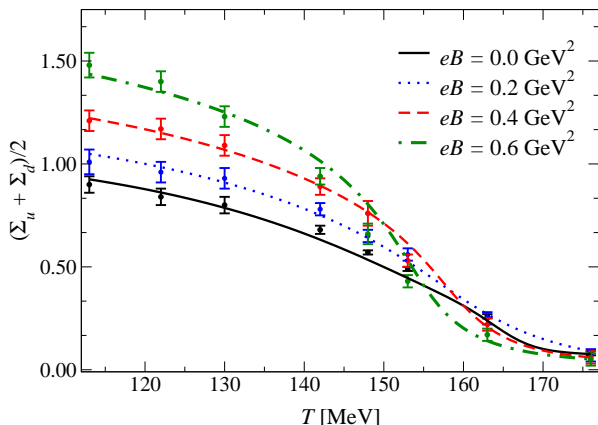


Fig. 1 Fit of the LQCD data [17] for the average quark condensate as a function of the temperature for several magnetic field values.

In figure 1 we show the thermal dependence of the average quark condensate for different values of B using the thermomagnetic dependent coupling $G(eB, T)$. The fit to the lattice data is very good. The figure clearly displays the IMC phenomenon for $eB \gtrsim 0.2 \text{ GeV}^2$ and $T \gtrsim 150 \text{ MeV}$. These results can be better understood with the aid of figure 2, which displays the predicted pseudocritical temperature T_{pc} as a function of eB . The inset in this figure shows that T_{pc} decreases with eB within the range $0.2 \text{ GeV}^2 < eB < 0.4 \text{ GeV}^2$. The predictions of the model compare fairly well with the

lattice data in the continuum extrapolation limit (blue band) [16] within the range of magnetic fields considered.

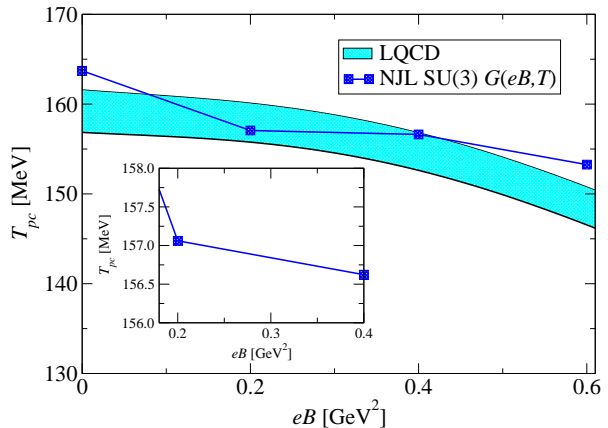


Fig. 2 Pseudocritical temperature as a function of the magnetic field compared with LQCD results in the extrapolation limit (blue band) [16].

Figure 3 displays the magnetic field dependence of the renormalized magnetization \mathcal{M}^r for three sets of temperature values. The top panel, for $T = 0$, shows results for three of the coupling values: $G(eB, T = 0)$ (blue dashed), $G = 1.835/\Lambda^2$ (yellow dotted) [57], and $G(0, 0)$ (green dot-dashed)—the six-quark coupling is the same in all cases, $K = 9.29/\Lambda^5$ [57]. The first two G -coupling values lead to fairly good agreement with the LQCD data of Ref. [32], whereas the agreement with the coupling $G(0, 0)$ is only good up to $eB \simeq 0.3 \text{ GeV}^2$. The figure also displays predictions from the hadron resonance gas (HRG) model [40], which also agree with LQCD data up to $eB \simeq 0.3 \text{ GeV}^2$ only. In the other two panels, we show results obtained with $G(eB, T)$ for $T = 113$ MeV (center panel) and $T = 176$ MeV (bottom panel). Very good agreement with the LQCD data of Ref. [40] is again observed for these temperatures.

For completeness, we present in figure 4 the model's predictions for the pressure, $P = -\Omega(T, eB)$, obtained in the MFIR and VMR schemes. The figure displays the magnetic field dependence of P for $T = 0$ (top panel) and $T = 176$ MeV (bottom panel). We do not show the results for $T = 113$ MeV, the temperature explored in figure 3, because they are very similar to those at $T = 0$. We compare results obtained with the running coupling, $G(eB, T)$, as well as with the fixed value of Ref. [57], indicated by HK in the figure—again, the six-quark coupling K is the same used above. The figure reveals that the pressure values predicted using $G(eB, T)$ are systematically lower than those where a T and B independent G has been

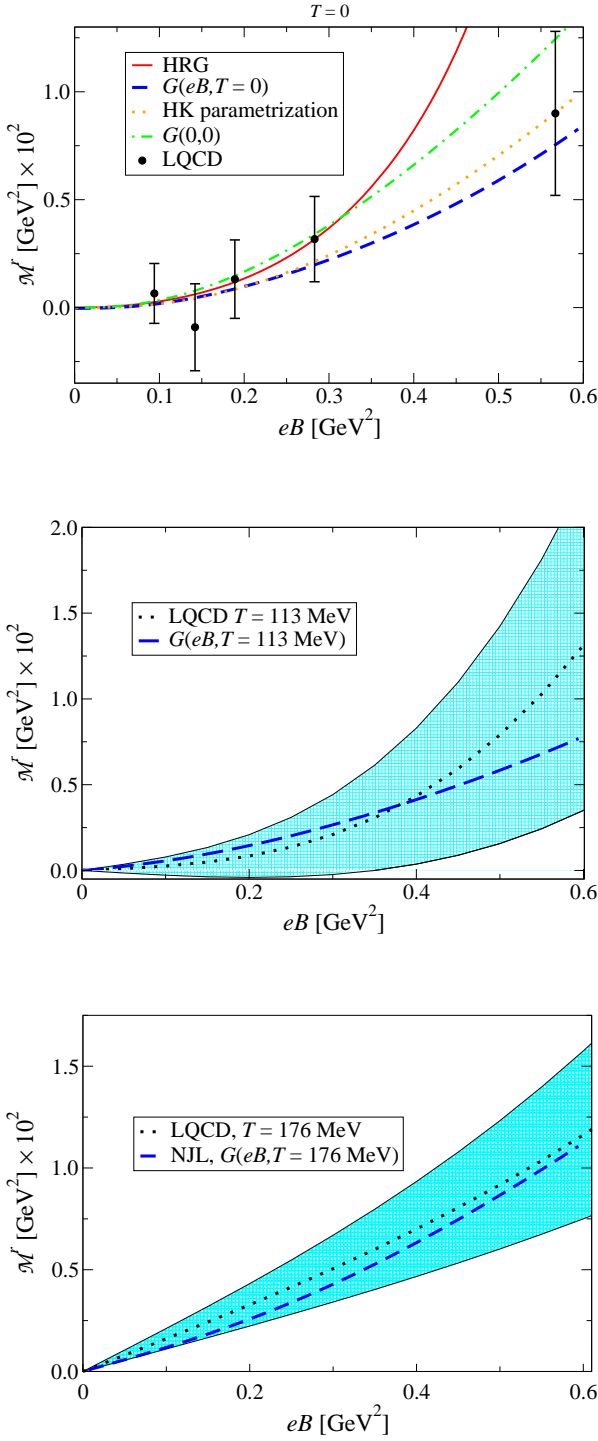


Fig. 3 Renormalized magnetization as function of magnetic field for three sets of temperatures: $T = 0$ (top panel), $T = 113$ MeV (center panel) and $T = 176$ MeV (bottom panel). The blue bands represent the error bands of the LQCD results black dotted line represents the fit for the LQCD results Ref. [40]).

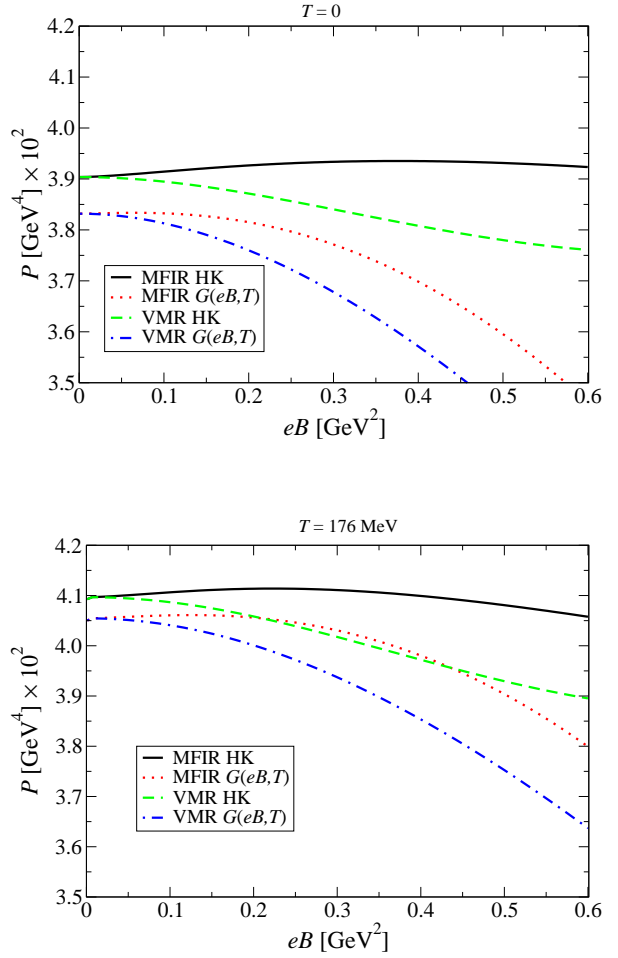


Fig. 4 Pressure ($P = -\Omega(T, eB)$) as function of the magnetic field for the temperatures $T = 0$ (top panel) and $T = 176$ MeV (bottom panel) in the MFIR and VMR schemes. Results obtained with $G(eB, T)$ and the vacuum coupling G (denoted HK) [57] (in both cases, the coupling K is the same).

used. This behavior is observed for both temperature values considered. Interestingly, the MFIR and VMR predictions have qualitatively different eB dependence for both values of T , a feature already pointed out in Ref. [54] for the SU(2) case: in the MIFR scheme, the eB dependence is nonmonotonic, P starts increasing and then decreases, whereas in the VMR scheme, P decreases monotonically with eB . This feature is observed for both temperature and coupling sets used. These results evince, now also for the SU(3) case, how the (divergent) mass independent terms present in the VMR scheme affect the B dependence of the pressure.

The importance of the mass independent terms present within the VMR can be further highlighted by examining the magnetization displayed in Fig. 5. The figure shows the results at $T = 0$ case (top panel) and $T = 176$ MeV (bottom panel) for both schemes with a fixed and a running four fermion coupling. One can

easily see that in the MFIR scheme we have $\mathcal{M} > 0$ for $eB \lesssim 0.3\text{GeV}^2$ in $T = 0$ and $eB \lesssim 0.2\text{GeV}^2$ in $T = 176 \text{ MeV}$ with fixed coupling. The MFIR results with $G(eB, T)$ show a similar behavior but $\mathcal{M} > 0$ is only observed at rather low B values. The VMR scheme shows $\mathcal{M} < 0$ for a fixed coupling at both temperatures considered (although the magnetization at these two temperature values increases when $T \gtrsim 0.3\text{GeV}^2$). The VMR scheme, with $G(eB, T)$, predicts a more dramatic (and completely monotonic) decrease of \mathcal{M} as the magnetic field increases. Highlighting, once again, the crucial role played by contributions which are subtracted within the MFIR method.

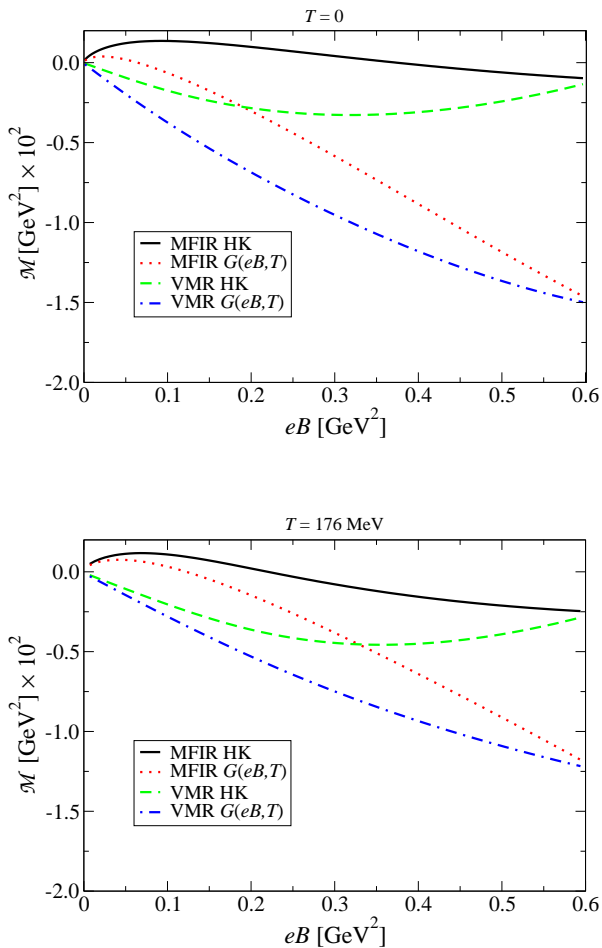


Fig. 5 Magnetization as function of the magnetic field for the fixed temperatures $T = 0$ (top panel) and $T = 176 \text{ MeV}$ (bottom panel).

5 Conclusions

In this work we extended the recently [54] proposed VMR scheme to describe magnetized strange quark matter within a three flavor NJL model framework. The thermomagnetic running of the four fermion coupling, $G(eB, T)$, was determined by fitting lattice QCD data for the quark condensate, reproducing in this way the inverse magnetic catalysis effect predicted by most lattice evaluations. When regulated with the VMR the thermodynamical potential presents mass independent terms which are usually subtracted in other schemes such as the MFIR. Since these extra terms are strongly B dependent their presence greatly impacts physical observables such as the magnetization. Despite the fact that the four dimensional NJL represents a nonrenormalizable theory one may, nevertheless, define a projected quantity, \mathcal{M}^r , which allows for a direct comparison with LQCD results in a satisfactory way (see Ref. [54] for details). Our results indicate a very good concordance with LQCD results with and without the thermomagnetic four fermion scalar coupling although IMC was present just when $G(eB, T)$ is considered, as expected. To show the importance of the mass independent terms in the thermodynamical potential, we have also compared the pressure and the magnetization as $\mathcal{M} = \partial P / \partial(eB)$ as function of the magnetic field in both MFIR and VMR schemes. The comparison with LQCD data has shown that the MFIR procedure is more sensitive to the variations of the magnetic field furnishing less reliable results. The present work shows that the VMR, originally proposed in the context of two flavors, can be readily generalized to the more realistic three flavor case. We have also demonstrated that when this regularization method is used in conjunction with an adequate thermomagnetic four fermion coupling the effective model is able to produce results which are in line with LQCD predictions. These include the IMC phenomenon as well as the paramagnetic character of the quark matter. A more complete analysis with the inclusion of the thermomagnetic dependence of the six fermion t'Hooft coupling is underway.

Acknowledgements This work was partially supported by Conselho Nacional de Desenvolvimento Científico e Tecnológico (CNPq), Grants No. 309598/2020-6 (R.L.S.F.), No. 304518/2019-0 (S.S.A.) No. 303846/2017-8 (M.B.P), and No. 309262/2019-4 (G.K.), No. 306615/2018-5 (V.S.T.); Coordenação de Aperfeiçoamento de Pessoal de Nível Superior - (CAPES) Finance Code 001 (W.R.T); Fundação de Amparo à Pesquisa do Estado do Rio Grande do Sul (FAPERGS), Grants Nos. 19/2551-0000690-0 and 19/2551-0001948-3 (R.L.S.F.); Fundação de Amparo à Pesquisa do Estado de São Paulo (FAPESP), Grant No. 2018/25225-9 (G.K.), No. 2019/10889-1 (V.S.T.); Fundo de Apoio ao Ensino, Pesquisa

e à Extensão (FAEPEX), Grant No. 3258/19 (V.S.T.). The work is also part of the project Instituto Nacional de Ciência e Tecnologia - Física Nuclear e Aplicações (INCT - FNA), Grant No. 464898/2014-5.

References

1. J. Rafelski, B. Muller, Phys. Rev. Lett. **36**, 517 (1976). DOI 10.1103/PhysRevLett.36.517
2. D.E. Kharzeev, L.D. McLerran, H.J. Warringa, Nucl. Phys. A **803**, 227 (2008). DOI 10.1016/j.nuclphysa.2008.02.298
3. V. Skokov, A. Illarionov, V. Toneev, Int. J. Mod. Phys. A **24**, 5925 (2009). DOI 10.1142/S0217751X09047570
4. R.C. Duncan, C. Thompson, Astrophys. J. Lett. **392**, L9 (1992). DOI 10.1086/186413
5. C. Kouveliotou, S. Dieters, T. Strohmayer, J. van Paradijs, G.J. Fishman, C.A. Meegan, K. Hurley, J. Kommers, I. Smith, D. Frail, T. Murakami, Nature **393**, 235 (1998). DOI 10.1038/30410
6. T. Vachaspati, Phys. Lett. B **265**, 258 (1991). DOI 10.1016/0370-2693(91)90051-Q
7. D. Grasso, H.R. Rubinstein, Phys. Rept. **348**, 163 (2001). DOI 10.1016/S0370-1573(00)00110-1
8. K. Fukushima, D.E. Kharzeev, H.J. Warringa, Phys. Rev. D **78**, 074033 (2008). DOI 10.1103/PhysRevD.78.074033
9. D.T. Son, A.R. Zhitnitsky, Phys. Rev. D **70**, 074018 (2004). DOI 10.1103/PhysRevD.70.074018
10. N. Yamamoto, Phys. Rev. Lett. **115**(14), 141601 (2015). DOI 10.1103/PhysRevLett.115.141601
11. D.E. Kharzeev, Prog. Part. Nucl. Phys. **75**, 133 (2014). DOI 10.1016/j.pnpnp.2014.01.002
12. X.G. Huang, Rept. Prog. Phys. **79**(7), 076302 (2016). DOI 10.1088/0034-4885/79/7/076302
13. J.O. Andersen, W.R. Naylor, A. Tranberg, Rev. Mod. Phys. **88**, 025001 (2016). DOI 10.1103/RevModPhys.88.025001
14. V.A. Miransky, I.A. Shovkovy, Phys. Rept. **576**, 1 (2015). DOI 10.1016/j.physrep.2015.02.003
15. A. Ayala, L.A. Hernández, M. Loewe, C. Villavicencio, ArXiv: 2104.05854.
16. G. Bali, F. Bruckmann, G. Endrődi, Z. Fodor, S. Katz, S. Krieg, A. Schafer, K. Szabo, JHEP **02**, 044 (2012). DOI 10.1007/JHEP02(2012)044
17. G. Bali, F. Bruckmann, G. Endrődi, Z. Fodor, S. Katz, A. Schäfer, Phys. Rev. D **86**, 071502 (2012). DOI 10.1103/PhysRevD.86.071502
18. G. Endrődi, M. Giordano, S.D. Katz, T. Kovács, F. Pittler, JHEP **07**, 007 (2019). DOI 10.1007/JHEP07(2019)007
19. H.T. Ding, C. Schmidt, A. Tomiya, X.D. Wang, Phys. Rev. D **102**(5), 054505 (2020). DOI 10.1103/PhysRevD.102.054505
20. A. Bandyopadhyay, R.L. Farias, Eur. Phys. J. Spec. Top. (2021). DOI 10.1140/epjs/s11734-021-00023-1
21. J.O. Andersen, ArXiv: 2102.13165.
22. Y. Nambu, G. Jona-Lasinio, Phys. Rev. **122**, 345 (1961). DOI 10.1103/PhysRev.122.345
23. Y. Nambu, G. Jona-Lasinio, Phys. Rev. **124**, 246 (1961). DOI 10.1103/PhysRev.124.246
24. R. Farias, K. Gomes, G. Krein, M. Pinto, Phys. Rev. C **90**(2), 025203 (2014). DOI 10.1103/PhysRevC.90.025203
25. R. Farias, V. Timóteo, S. Avancini, M. Pinto, G. Krein, Eur. Phys. J. A **53**(5), 101 (2017). DOI 10.1140/epja/i2017-12320-8
26. M. Ferreira, P. Costa, O. Lourenço, T. Frederico, C. Providência, Phys. Rev. D **89**(11), 116011 (2014). DOI 10.1103/PhysRevD.89.116011
27. M. Ferreira, P. Costa, D.P. Menezes, C. Providência, N. Scoccola, Phys. Rev. D **89**(1), 016002 (2014). DOI 10.1103/PhysRevD.89.016002. [Addendum: Phys.Rev.D 89, 019902 (2014)]
28. G. Endrődi, G. Markó, JHEP **08**, 036 (2019). DOI 10.1007/JHEP08(2019)036
29. J. Moreira, P. Costa, T.E. Restrepo, Phys. Rev. D **102**(1), 014032 (2020). DOI 10.1103/PhysRevD.102.014032
30. J. Moreira, P. Costa, T.E. Restrepo, Eur. Phys. J. A **57**(4), 123 (2021). DOI 10.1140/epja/s10050-021-00440-9
31. A. Martínez, A. Raya, Nucl. Phys. B **934**, 317 (2018). DOI 10.1016/j.nuclphysb.2018.07.008
32. G. Bali, F. Bruckmann, G. Endrődi, F. Gruber, A. Schäfer, JHEP **04**, 130 (2013). DOI 10.1007/JHEP04(2013)130
33. G. Endrődi, JHEP **04**, 023 (2013). DOI 10.1007/JHEP04(2013)023
34. C. Bonati, M. D'Elia, M. Mariti, F. Negro, F. Sanfilippo, Phys. Rev. Lett. **111**, 182001 (2013). DOI 10.1103/PhysRevLett.111.182001
35. C. Bonati, M. D'Elia, M. Mariti, F. Negro, F. Sanfilippo, Phys. Rev. D **89**(5), 054506 (2014). DOI 10.1103/PhysRevD.89.054506
36. P. Adhikari, J.O. Andersen, ArXiv: 2102.01080.
37. A.N. Tawfik, A.M. Diab, M.T. Hussein, J. Exp. Theor. Phys. **126**(5), 620 (2018). DOI 10.1134/S1063776118050138
38. C.P. Hofmann, ArXiv: 2012.06461.
39. C.P. Hofmann, ArXiv: 2103.04937.
40. G.S. Bali, F. Bruckmann, G. Endrodi, A. Schafer, Phys. Rev. Lett. **112**, 042301 (2014). DOI 10.1103/

- PhysRevLett.112.042301
41. D. Ebert, K. Klimenko, Nucl. Phys. A **728**, 203 (2003). DOI 10.1016/j.nuclphysa.2003.08.021
 42. D. Ebert, K. Klimenko, M. Vdovichenko, A. Vshivtsev, Phys. Rev. D **61**, 025005 (2000). DOI 10.1103/PhysRevD.61.025005
 43. S.S. Avancini, R.L. Farias, N.N. Scoccola, W.R. Tavares, Phys. Rev. D **99**(11), 116002 (2019). DOI 10.1103/PhysRevD.99.116002
 44. D.C. Duarte, P. Allen, R. Farias, P.H.A. Manso, R.O. Ramos, N. Scoccola, Phys. Rev. D **93**(2), 025017 (2016). DOI 10.1103/PhysRevD.93.025017
 45. P.G. Allen, A.G. Grunfeld, N.N. Scoccola, Phys. Rev. D **92**(7), 074041 (2015). DOI 10.1103/PhysRevD.92.074041
 46. D. Menezes, M. Benghi Pinto, S. Avancini, A. Perez Martinez, C. Providência, Phys. Rev. C **79**, 035807 (2009). DOI 10.1103/PhysRevC.79.035807
 47. D. Menezes, M. Benghi Pinto, S. Avancini, C. Providência, Phys. Rev. C **80**, 065805 (2009). DOI 10.1103/PhysRevC.80.065805
 48. S.S. Avancini, D.P. Menezes, M.B. Pinto, C. Providência, Phys. Rev. D **85**, 091901 (2012). DOI 10.1103/PhysRevD.85.091901
 49. S.S. Avancini, R.L.S. Farias, M. Benghi Pinto, W.R. Tavares, V.S. Timóteo, Phys. Lett. B **767**, 247 (2017). DOI 10.1016/j.physletb.2017.02.002
 50. S.S. Avancini, V. Dexheimer, R.L.S. Farias, V.S. Timóteo, Phys. Rev. C **97**(3), 035207 (2018). DOI 10.1103/PhysRevC.97.035207
 51. S.S. Avancini, R.L. Farias, W.R. Tavares, Phys. Rev. D **99**(5), 056009 (2019). DOI 10.1103/PhysRevD.99.056009
 52. M. Coppola, P. Allen, A. Grunfeld, N. Scoccola, Phys. Rev. D **96**(5), 056013 (2017). DOI 10.1103/PhysRevD.96.056013
 53. A. Bandyopadhyay, R.L.S. Farias, B.S. Lopes, R.O. Ramos, Phys. Rev. D **100**(7), 076021 (2019). DOI 10.1103/PhysRevD.100.076021
 54. S.S. Avancini, R.L.S. Farias, M.B. Pinto, T.E. Restrepo, W.R. Tavares, Phys. Rev. D **103**(5), 056009 (2021). DOI 10.1103/PhysRevD.103.056009
 55. U. Vogl, W. Weise, Prog. Part. Nucl. Phys. **27**, 195 (1991). DOI 10.1016/0146-6410(91)90005-9
 56. S.P. Klevansky, Rev. Mod. Phys. **64**, 649 (1992). DOI 10.1103/RevModPhys.64.649
 57. T. Hatsuda, T. Kunihiro, Phys. Rept. **247**, 221 (1994). DOI 10.1016/0370-1573(94)90022-1
 58. T. Kunihiro, T. Hatsuda, Phys. Lett. B **206**, 385 (1988). DOI 10.1016/0370-2693(88)91596-1. [Erratum: Phys.Lett.B 210, 278–278 (1988)]